Available online at www.sciencedirect.com
SCIENCE DIRECT
Thermochimica Acta 443 (2006) 159–172
thermochimica acta
www.elsevier.com/locate/tca

Confined rapid thermolysis/FTIR/ToF studies of imidazolium-based ionic liquids

Arindrajit Chowdhury, Stefan T. Thynell *

Department of Mechanical and Nuclear Engineering, The Pennsylvania State University, University Park, PA 16802, USA

Received 14 December 2005; received in revised form 4 January 2006; accepted 6 January 2006
Available online 21 February 2006

Abstract

Rapid scan FTIR spectroscopy and time-of-flight (ToF) mass spectrometry were utilized to study thermal decomposition of three imidazolium-based ionic liquids, with 1-ethyl-3-methyl-imidazolium (emim) as the cation, and NO_3^-, Cl^-, and Br^- as the anions. The thermal decomposition involved heating rates of 2000 K/s and temperatures to 435 °C in an ambient inert gas at 1 atm. Using sub-milligram quantities of each compound, examinations of the evolution of gas-phase species revealed that the most probable sites for proton transfer and subsequent secondary reactions were primarily the methyl group and secondarily the ethyl group. The ring appeared to remain intact, as there was no evidence of the formation of HCN, imines or related products. The most reactive compound is [emim]NO_3, since the nitrate group served as a strong oxidizer and reacted strongly with the methyl/ethyl groups at the elevated temperatures to produce common final products from combustion.

Keywords: Ionic liquids; Thermal decomposition; FTIR spectroscopy; ToF mass spectrometry

1. Introduction

Ionic liquids are a unique class of ionic compounds with melting points below the boiling point of water. Room temperature ionic liquids (RTILs) are a sub-category of ionic liquids with melting points below the ambient temperature. While the first room temperature energetic ionic liquid, [$CH_3CH_2NH_3$]–[NO_3], with a melting point of only 12 °C was reported in 1914 by Walden [1], the modern era of ionic liquids started with the synthesis of 1-butylpyridinium chloride-aluminum(III) chloride mixture by Osteryoung et al. [2]. The reducible nature of *N*-alkyl-pyridinium cations in basic solutions led to a search for more stable cations. Wilkes [3] studied a wide range of heterocyclic cations with quaternary *N*-atoms and found the dialkyl-imidazolium cation to be the most suitable one. Further studies by Fannin et al. [4] revealed that the 1-ethyl-3-methyl-imidazolium (emim) cation was an excellent compromise between ease of synthesis and desirable properties. However, chloroaluminate ionic liquids, prepared by mixing aluminium chloride with dialkyl-imidazolium chlorides, were found to be hygroscopic. This led to the search for anions that would yield ionic liquids stable towards hydrolysis at room temperature, culminating in the discovery of tetrafluoroborate, hexafluorophosphate, nitrate, sulfate and acetate salts by Wilkes and Zaworotko [5]. The last decade has sparked a significant interest in synthesis and analysis of new ionic liquids, with the focus being on imidazoles, triazoles, tetrazoles and other nitrogen-containing heterocyclic compounds and their salts.

1.1. Thermodynamic properties and behavior

The most significant characteristic of RTILs is their low melting points and extremely large liquidus range. The phase diagram of [emim]Cl–$AlCl_3$ shows that melting points below −90 °C are possible [4,6]. These properties can be attributed to absence of strong hydrogen bonding [5,7], highly asymmetric cations paired with bulky anions leading to poor packing efficiencies, charge delocalization on the cation, and addition of solvent-like tails [8–10]. They also display a remarkably low vapor pressure, related to their high cohesive energy density [11]. The above-mentioned properties make them environmentally benign replacements for noxious organic solvents [12,13]. High electrical conductivity, a wide electrochemical window as well as excellent thermal and chemical stability facilitate their use as

* Corresponding author. Tel.: +1 814 865 1345; fax: +1 814 865 6696.
E-mail address: Thynell@psu.edu (S.T. Thynell).

0040-6031/$ – see front matter © 2006 Elsevier B.V. All rights reserved.
doi:10.1016/j.tca.2006.01.006

electrolytic solvents for catalytic reactions [14–16] as well as the potential application to solar cells and fuel cells. Besides their conventional application as solvents, the low vapor pressure, high energy density and high solubility in many polar solvents have established ionic liquids as potential fuels and monopropellants [17].

1.2. Previous research on decomposition of energetic imidazoles and salts

For efficient use and safety concerns, an understanding is needed about the temperature dependence and chemical kinetics of their thermal decomposition under high heating rates. Information available on the kinetics of the thermal decomposition of imidazoles and their salts is relatively sparse in the literature. However, studies on solubilities, vapor–liquid equilibria, molar volumes and specific heat are available for some imidazolium salts [18–20]. No chemical kinetics on thermal decomposition appear to be available on the energetic imidazolium compounds, such as [emim]-X, with X as NO_3^-, $C1O_4^-$, $N(NO_2)_2^-$. Except one, most studies on decomposition have been carried out using thermogravimetric techniques [10,21–26].

Pyrolysis of a wide range of 1,3-disubstituted imidazolium salts, R_1R_2Imidazolium X (R_1, R_2 = methyl, ethyl, propyl, isopropyl, butyl, benzyl, vinyl, phenyl, and allyl; X = Cl^-, Br^-, I^-, Ph_4B^- and ClO_4^-) was carried out by Chan et al. [27]. Barring the Ph_4B^- and ClO_4^- salts, all the other [emim]-X compounds, when subjected to a temperature of 220–260 °C for 0.5–1.5 h under vacuum, formed 1-substituted imidazoles. Quantitative analysis of the products was carried out by NMR spectroscopy and gas chromatography. 1-Ethylimidazole was found to dominate the products over 1-methylimidazole, and no traces of HX were detected. Similar studies on [emim]-X salts (X = bis-(methanesulfonyl)amide, bis-(trifluoromethanesulfonyl)amide) by Baranyai et al. [28] yielded 1-ethylimidazole as the major degradation product and 1-methylimidazole as the minor one. Again, no acids corresponding to the anions were detected. The predominance of 1-ethylimidazole during decomposition was attributed to an S_N2 process.

Bônhote et al. [10] examined the thermal stability of a wide variety of 1,3-dialkyl-imidazolium cations and hydrophobic anions, which included trifluoromethanesulfonates (TfO^-), bis((trifluoromethanesulfonyl)amides (Tf_2N^-) and trifluoroacetates (TA^-). The melting points of many of these salts were as low as −30 to −50 °C but their correlation to chemical composition was difficult. For heating rates of 10 °C/min, the [emim]TfO and [emim]Tf2N were stable up to 400 °C, but decomposed rapidly between 440 and 480 °C. However, [emim]TA initiated its decomposition at 150 °C and continued until reaching 250 °C, when nearly all the material was converted to gaseous products. The same results were obtained with either air or N_2. Correlation of mass loss with evolved species was not discussed.

Ngo et al. [21] used TGA/SDTA and DSC to study the thermal stability of a wide variety of imidazolium cations as well as organic and inorganic anions at heating and cooling rates of 10 °C/min. The thermal decomposition behavior varied considerably with salt structure, as well as pan composition. The aluminum pan catalyzed the decomposition, requiring the use of alumina pans. Nonetheless, many interesting findings were obtained. The thermal stability was enhanced with increased substitution on the imidazolium cation, i.e. replacing the ring hydrogens with methyl or *N*-propyl groups enhanced stability. The effect on stability was observed when the C(2) hydrogen was removed due to the acidity of the proton. Additionally, [emim] halides (Cl^-, Br^- and I^-) exhibited the lowest temperature for the onset of decomposition (280–310 °C), and the salts showed similar thermal behavior in O_2 or N_2 environments.

Egashira et al. [24] examined the thermal stability of three different [emim] salts with either individual anions, such as $CF_3SO_3^-$ or BF_4^-, or mixture of different anions, such as $CF_3SO_3^-$ or BF_4^- with bis(tetrafluoromethanesulfonyl)imide ($TFSI^-$). A heating rate of 5 °C/min in an Ar environment was employed. The thermogravimetric data for $[emim](BF_4)_{0.5}(TFSI)_{0.5}$ were essentially the arithmetic average of the data from for [emim]BF_4 and [emim]TFSI. However, the data for $[emim](CF_3SO_3)_{0.5}(TFSI)_{0.5}$ were more similar to [emim]CF_3SO_3 than to [emim]TFSI.

Bhattacharjee and Choudhury [25] studied several imidazole complexes of Cu(II). For the $(H_2Im)_4[CuF_6]$ salt, thermogravimetric studies revealed 66% weight loss over the temperature range from 250 to 350 °C by a release of (3HIm + 3HF + F_2) in an endothermic process. From 400 to 700 °C, (H_2ImF) was released also in an endothermic process; a Cu_2O residue remained. The thermogravimetric data on imidazole complexes revealed similar processes occurring in either two or three endothermic stages.

Minier et al. [29] studied the solid-phase thermal decomposition of 2,4-dinitro-imidazole (DNI) using thermogravimetric and mass spectrometric techniques. The first stage of decomposition was found to be related to the presence of water and impurities in the DNI. As this "early decomposition" was ending, an induction period began with the evolution of CO_2 and NO. This stage was followed by an auto-acceleratory stage where the major products included CO_2, CO, NO, N_2, HNCO and H_2O. Finally, the residue from this stage decomposed. It was also postulated that the decomposition of DNI involved multiple pathways including a nitro-nitrite rearrangement, followed by bond scission to form NO, and then an N–C bond scission, which opened the ring. Intra- and inter-molecular hydrogen abstraction was also believed to be one of the initiation steps.

The temperatures defining onset of the thermal decomposition of a broad range of energetic ionic liquids have recently been established by thermogravimetric methods [30–32]. Nitrates and perchlorates of azido and nitro derivatives of imidazole, 1,2,4-triazole and substituted derivatives of tetrazoles were synthesized and their decomposition points recorded under a heating rate of 10 °C/min. Nitrate salts of substituted imidazoles, triazoles and tetrazoles were found to have a lower thermal stability than the perchlorate salts in general. Decomposition temperatures of substituted imidazoles were found to decrease with increased substitution of ring hydrogens. As a result, 1,3-dimethyl-5-nitroimidazolium nitrate (174 °C) was found to be more stable than 1,3,5-trimethyl-5-nitroimidazolium nitrate (166 °C), which in turn was found to be more stable than 1-ethyl-2,3-dimethyl-5-nitroimidazolium nitrate (146 °C). How-

ever, such a relationship was lacking among the perchlorate salts of the same category, where 1,3,5-trimethyl-5-nitroimidazolium perchlorate (307 °C) was found to be the most stable salt. Similar trends were observed among the triazole and tetrazole salts.

Recently, the slow thermal decomposition characteristics of several energetic ionic liquids were examined using thermogravimetric analysis and differential scanning calorimetry, coupled with IR spectroscopy and mass spectrometry [33]. Decomposition of the 1,5-diamino-4-methyl-1*H*-tetrazolium nitrate involved methyl group transfer to form $MeONO_2$, rather than proton transfer to form HNO_3. At heating rates of 10 °C/min, this ionic liquid began to decompose at 181 °C, and showed a peak heat release rate at 200 °C.

Finally, IR laser ablation of 1,3-disubstituted imidazolium salts, R_1R_2Imidazolium X (R_1 = methyl, R_2 = methyl, ethyl, butyl and hexyl; X = Cl^-, NO_3^- and $CH_3SO_4^-$) was studied using time-of-flight mass spectrometry by Baer et al. [34]. Unlike previous studies, the heating rates employed were 10^8–10^{13} K/s. The internal temperature of the ablated vapor plume was measured to be 450–500 °C by an ethylene glycol thermometer. Vacuum photoionization was utilized to detect the neutral species. Approximately 100 mg of the ionic liquids studied was ablated and 99% of the sample was found to be vaporized to form nano- or micro-droplets. The remaining 1% was comprised mainly of stable di-substituted imidazoles, formed by expulsion of HCl from the imidazolium salt. About 0.1% was found to be the gas-phase parent molecules, R_1R_2Imidazolium X.

1.3. Current issues and objectives of this work

It is well-known that some energetic materials exhibit several important chemical kinetic decomposition pathways, requiring the use of both slow and rapid heating of the energetic material [35]. The concluded discussion shows that decomposition of disubstituted imidazolium salts follows different pathways under different heating rates—low heating rates lead to monosubstituted imidazoles, whereas high heating rates lead to disubstituted imidazoles. However, the pathways are generally difficult to elucidate, since they are believed to occur in the condensed phase. Despite the potential complexity involved in predicting the characteristics of condensed-phase reactions, several observations can be made based on decomposition of organic salts and related molecules. First, multiple initiation reactions occur including homolysis and proton transfer. Second, competing reaction pathways exist with relative rates dependent on temperature and heating rates. Third, the reactions tend to be auto-catalytic. Fourth, reactivity varies with the structure of the cation and anion. Fifth, the reactions are sensitive to the presence of catalysts. And sixth, products with high molecular weights may be formed due to recombination of intermediates formed on ring scission.

The objective of this study is to identify initiation and secondary reactions in the condensed phase for ionic liquids, that lead to ignition and combustion under high heating rates and elevated temperatures, using Fourier transform infrared (FTIR) spectroscopy and time-of-flight (ToF) mass spectrometry (MS). Of particular interest is to identify the proton transfer mechanism. The use of two independent diagnostic tools enables comparison of results and eliminates ambiguity. Temperatures employed to decompose the ionic liquids can be accurately controlled during the process. The model energetic ionic liquid chosen for this purpose is [emim]-X with X as NO_3^-, Cl^- and Br^-, as shown in Fig. 1.

2. Experimental approach

2.1. Experimental setup

The technique utilized to study the products formed under rapid decomposition of a material is referred to as confined rapid thermolysis (CRT)/FTIR/ToFMS. Using this technique, the thermal decomposition is limited to a volume confined between two heated, parallel surfaces. By using a small sample size compared to the volume, it is possible to study liquids that may otherwise largely boil off rather than decompose. The setup is composed of a constant pressure chamber, a Bruker IFS 66/S FTIR spectrometer and a commercially available ToF mass spectrometer. A three-dimensional view of the chamber, including a cut that exposes the sample holder, is shown in Fig. 2. The sample holder is designed to be lifted by the bottom heater to enclose the sample between the two heaters. Two ports are provided on the chamber, one serves as an inlet to the purge gas and the other exhausts decomposition products and the purge gas stream. The constant pressure chamber, resting on a rigid frame, has a height of 27.5 cm and an inner diameter of 5 cm approximately. The CRT/FTIR technique has been described in detail in a previous work [36].

The rapid thermolysis is achieved by using two heaters: a stationary top heater and a mobile bottom heater. In both heaters, isothermal conditions are established by using high-watt density cartridge heaters (*Omega CIR-1014/120 V*) and controlled by proportional-integral-derivative (PID) controllers (*Omega CN8500*). Both heaters are sheathed in copper rods, 53 mm in height and 15.6 mm in diameter. There are two auxiliary systems, a pneumatic piston-cylinder (Motion Controls) for lifting

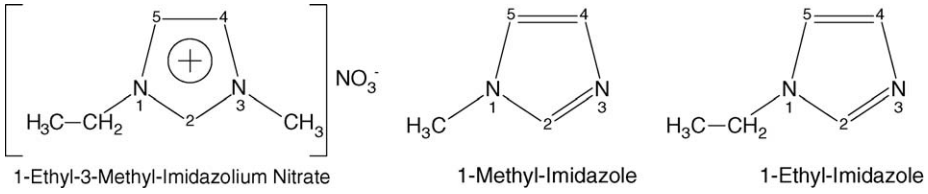

Fig. 1. Structures of 1-ethyl-3-methyl-imidazolium nitrate, 1-methyl-imidazole and 1-ethyl-imidazole.

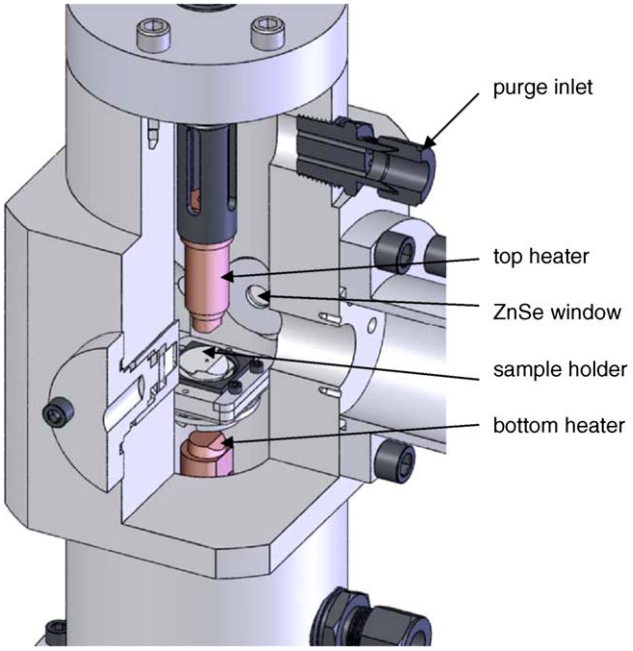

Fig. 2. Three-dimensional view of the high-pressure thermolysis chamber, exposing the sample holder, upper and lower heater, and the ZnSe windows through which the modulated beam of the FTIR propagates.

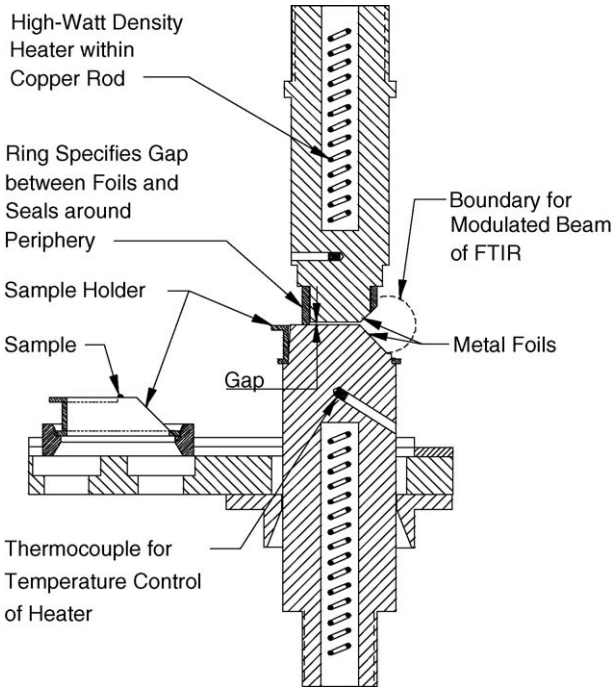

Fig. 3. Cross-sectional view when the two isothermal heaters are in contact, as well as initial sample holder position.

the bottom heater and a purge gas system. The purging system using an inert gas serves a dual purpose. One, it purges the chamber of the decomposition products and prevents recirculation of products into the path of the modulated FTIR beam, and two, it prevents oxidation of the copper rods at elevated temperatures. The temperature of the cartridge heaters is monitored and controlled by two 75 μm K-type thermocouples embedded in the copper sheaths of the heaters.

To achieve rapid thermolysis, defined as an event that occurs within 5 s, temperatures of above 400 °C are used. The experimental procedure is as follows: the heaters are brought up to the pre-set temperature. Approximately 0.5 mg of the ionic liquid is placed on the sample holder. As shown in Fig. 2, the sample holder is a hollow cylindrical ring with a thin foil attached on top. Though it is possible to utilize different types of foils, an 11 μm thick aluminum foil is used to minimize conductive heat transfer resistance. The sample holder is then placed over the guiding tube for the bottom heater and the bottom heater is raised by the pneumatic piston-cylinder. The sample holder is brought in contact with the ring retaining an aluminum foil over the top heater. This ring also defines and seals a gap of approximately 300 μm between the two heaters. The final position of the sample holder and the two heaters is shown in Fig. 3. A rectangular slit, 8.25 mm × 300 μm, is left open in the gap for gases generated during decomposition of the sample to gain access to the FTIR beam or to the orifice port on the vacuum chamber.

2.2. FTIR spectrometer

The gaseous products evolve into the FTIR beam passing through two ZnSe (or KRS-5) windows, which are offset by 0.313 in. from the center of the chamber, offering a spectral coverage of 500–10,000 cm^{-1}. This wide range is truncated using a germanium coated KBr beamsplitter and a mercury-cadmium-telluride detector to the mid-IR range of 600–5000 cm^{-1}. The gases evolved during the thermolysis are detected, identified and quantified using FTIR transmission spectroscopy. The spectra are acquired with a spectral resolution of 2 cm^{-1} and a temporal resolution of 50 ms.

2.3. ToF mass spectrometer

A low-pressure chamber with identical heater configurations is utilized for acquiring the ToF mass information at a high temporal resolution. The ToF MS system (Model D-677 from R.M. Jordan, http://www.rmjordan.com) is equipped with a 1 m flight tube and a 44 mm microchannel plate (MCP) detector. Here, the recharging of the MCP detector limits the temporal resolution to about 1 ms. The vacuum system is differentially pumped using a Leybold DIP8000 diffusion pump in the first stage, a Leybold TW700 turbomolecular pump in the second stage and a Leybold TMP151 turbomolecular pump as well as two Varian Starcell 75 ion pumps in the third stage; four backing pumps are also used. Typical pressures are 10^{-4} Torr in the first stage, 10^{-6} Torr in the second stage and 10^{-7} Torr in the third stage. Molecular beam sampling from atmospheric pressure gases is performed using a 100 μm orifice plate attached to the first stage, a 1 mm diameter Ni skimmer (manufactured in-house by electroplating) attached to the second stage and a vertically translatable 0.5 mm × 12 mm slit attached to the entrance of the third stage. A schematic is shown in Fig. 4. The distance between the orifice plate and the electron beam in the flight tube is 0.279 m. Electron impact ionization is set at 70 eV, resulting fragmenta-

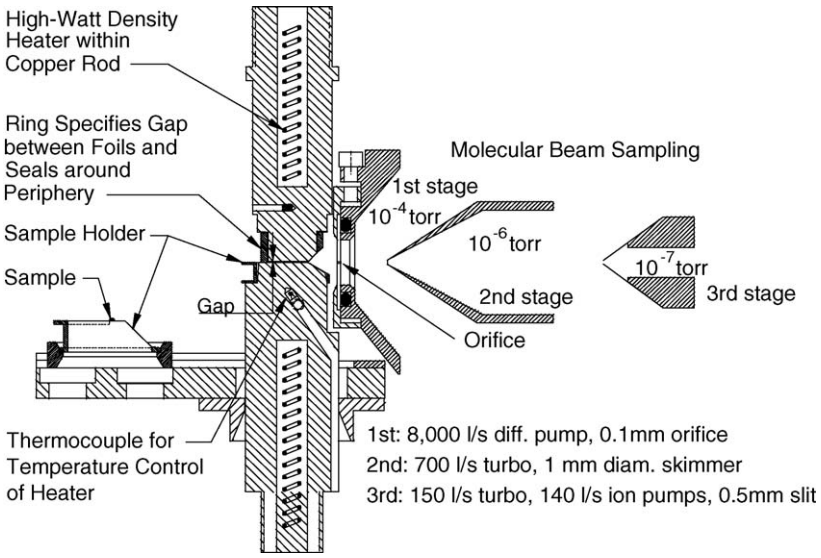

Fig. 4. Sampling of evolved gaseous products occurs via the 100 μm diameter orifice port located on the first stage of the vacuum chamber.

tion of molecules, but allowing comparison with mass spectral and related data bases [37]. The electron beam interacts with the molecular beam during a period of 3 μs, after which extraction of positive ions occurs as a 250 V voltage difference is applied between the grid plates; the overall potential is normally set at 2.5 kV. Data acquisition at 1 GHz is PC-based using the 8-bit PDA1000 PCI-board (www.Signatec.com), which has 256MB of on-board memory and a 3-dB bandwidth of 0.5 GHz.

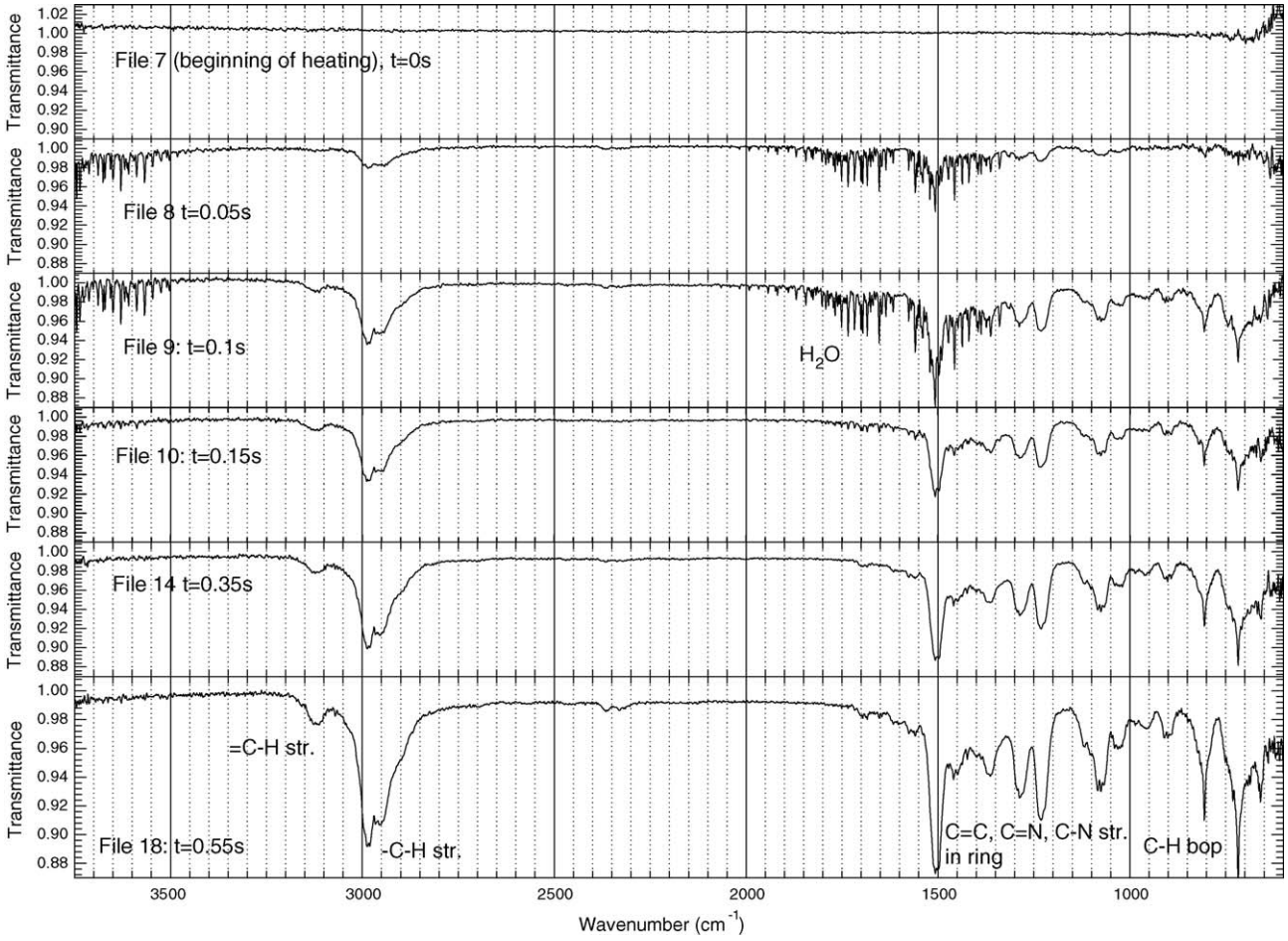

Fig. 5. FTIR spectra showing the evolution of species from rapid thermolysis of [emim]Cl at 425 °C and 1 atm N_2.

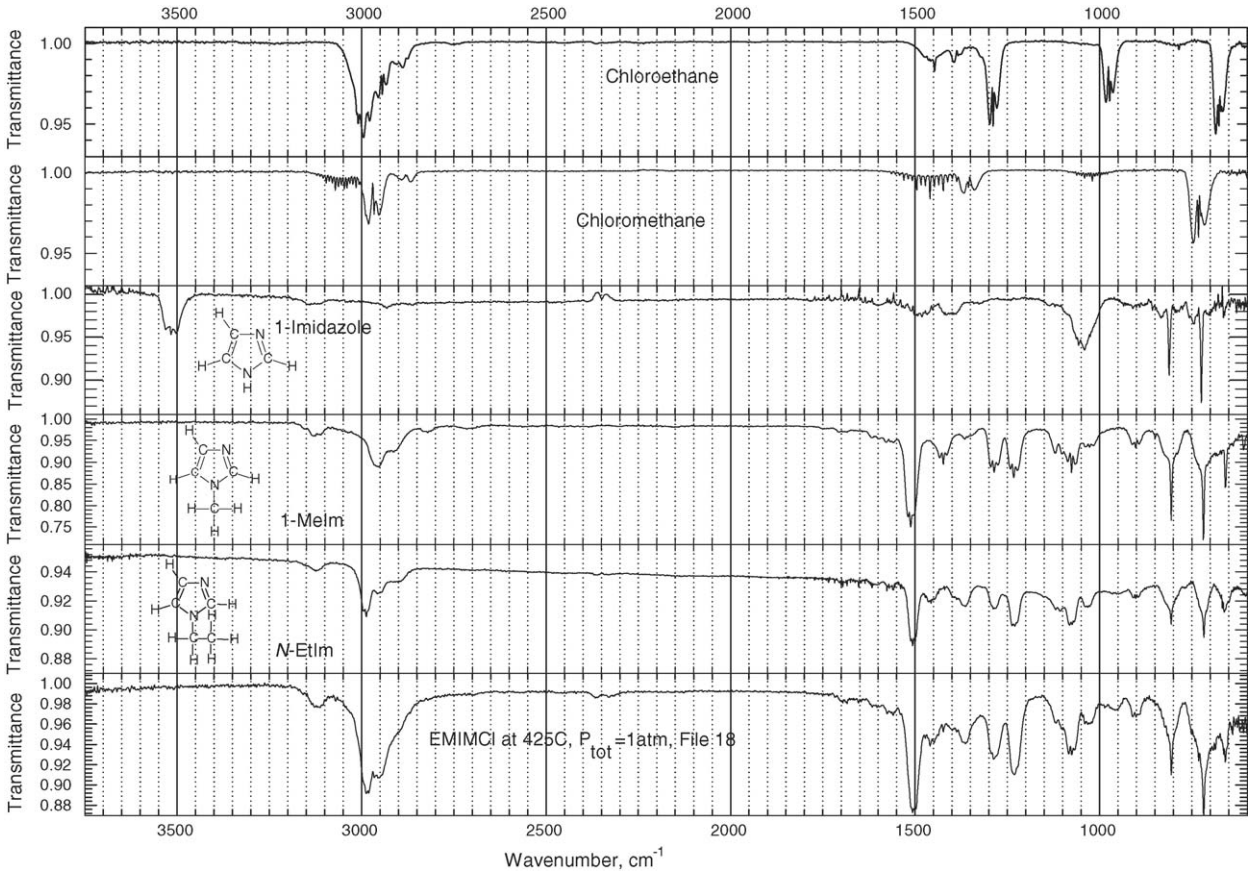

Fig. 6. FTIR spectra of [emim]Cl, *N*-EtIm, 1-MeIm, 1-imidazole, chloromethane and chloroethane for identification of thermolysis products.

The MCP output signal is inverted and amplified 3.5× using a THS3201 amplifier from Texas Instruments. Time-to-mass scaling is sufficient using the expressions $m = a(t - t_0)^2$, where the two constants for each mass spectrum are obtained from known positions of helium and argon.

3. Results and discussion

3.1. Thermal decomposition of [emim]Br and [emim]Cl

Numerous screening attempts were made in order to identify the temperature at which rapid thermolysis occurred of the two imidazolium halides [emim]Br and [emim]Cl. These two salts have melting points of 76.5 and 77–79 °C, respectively. Evolution of gas-phase species at a rapid rate began to occur at temperatures near 390 °C; at 350 °C, no gaseous species were detected during a 5 s time interval. The sample remained on the foil, and it showed no discoloration. Using a sample size of approximately 0.5 mg, Fig. 5 shows the evolution of species from thermolysis of [emim]Cl at a temperature of 425 °C. As the two heaters came in contact, one notes a slight baseline shift in the spectral transmittance that serves as the indicator for the beginning of heating. Both ionic liquids are also very hygroscopic, which makes it very difficult to study the thermolysis behavior of pure compounds. Fig. 5 shows that the band features evolve quite evenly and very early. Starting near 3125 cm^{-1}, the =C–H stretching frequency is clearly observed in file 9. Near 2980 and 2950 cm^{-1}, –C–H stretching frequencies are also observed. The absence of an N–H stretch near 3500 cm^{-1} is also noted. In the range from 1500 to 600 cm^{-1}, the spectra are very complex and definite assignment is difficult without the use of calibration compounds.

To aid in the interpretation of the acquired spectra, Fig. 6 shows the typical spectral transmittances of 1-*H*-methylimidazole (1-MeIm), 1-*H*-imidazole (1-Im), *N*-ethylimidazole (*N*-EtIm), chloromethane (MeCl) and chloroethane (EtCl). The *N*-EtIm of 99.5% purity was acquired from www.vwr.com and used without further purification. The other compounds (>98% purity) were acquired from Sigma–Aldrich and also used without further purification.

The 1-MeIm exists as a liquid under standard conditions, with a melting point of −60 °C and a boiling point of 198 °C. The FTIR spectrum of 1-MeIm in Fig. 6 was acquired in the thermolysis test rig at 281 °C and 1 atm pressure under a nitrogen environment. A comparison between the known and observed rovibrational frequencies of various bonds in the molecule is presented in Table 1. All the vibrational modes in the imidazole molecule are IR active and have been well-documented by Tatara et al. [38] using computational methods. The assignment of frequencies below 1600 cm^{-1} was in excellent agreement with previous work done by Sadlej et al. [39]. The =C–H in-plane stretching vibrational frequency was slightly over-

Table 1
Comparison of rovibrational frequencies of 1-MeIm with standard data published in the literature [38–40]

Description	Frequency (cm^{-1}) (predicted)	Frequency band (cm^{-1}) (experimental)
=C–H str	3273/3245/3242	3200–3100
C–H str in methyl group	2975–2950	2980–2940
C=C str	1555	1550–1475
C=C, C=N str, C-H bip	1496	1550–1475
C=C, C=N str	1430	1440–1400
C–N str, C–H bip	1282	1300–1200
C=C, C=N str	1092	1100–1060
C–N(1)-C bip, C–H bip	1073	1100–1060
C–N(1)-C bip	908	930–880
C–H bop	808	780–850
C–H bop	729	740–700

predicted. However, the C=C, C=N and C–H bending-in-plane (bip) stretching vibrational frequency bands matched perfectly with the computed frequencies. The C–N(1)–C bip and the C–H bending-out-of-plane (bop) frequencies were also well-predicted. In addition to the imidazole ring, the frequency of the C–H stretch in the terminal methyl group was confirmed in a review of available data by Socrates [40].

Examination of the spectral transmittances in Fig. 6 of the *N*-EtIm and 1-Im reveals significant similarities with 1-MeIm, in particular for the *N*-EtIm. The *N*-EtIm is a liquid at room temperature and has a listed boiling temperature of 79–81 °C; studies here were conducted at 200 °C. 1-Im has a melting point of 89–91 °C and a boiling temperature of 257 °C; studies here were conducted at 281 °C. Clearly, the –C–H stretching frequency near 2980 cm^{-1} must be associated with the carbon atom in the ethyl group attached to the ring nitrogen. Many of the observed bands from 1600 to 600 cm^{-1} are associated with various vibrational modes of the ring as discussed previously; strengths of bands associated with either the ethyl or methyl group appear to be moderately weak at best. Differences between 1-MeIm and *N*-EtIm are noted in the region from 1460 to 1325 cm^{-1}. Additionally, the heterocyclic compounds were also subjected to thermolysis at higher temperatures, but it is clear that evaporation dominates and decomposition does not occur within the short residence time within the confined volume between the two heaters. The MeCl and EtCl are also highly stable compounds, as revealed in numerous decomposition studies [41]. In addition, the tests carried out using the FTIR spectrometer were found to be highly repeatable, with variations between transmittances staying below 15% for any compound. The variations were found to be largely caused by the difficulty in accurately selecting the exact mass due to the crystalline nature of the studied compounds.

Based on the results in Figs. 5 and 6, the thermolysis behavior of [emim]Cl involves two pathways. The first pathway involves the formation of MeCl and *N*-EtIm, whereas the second path-

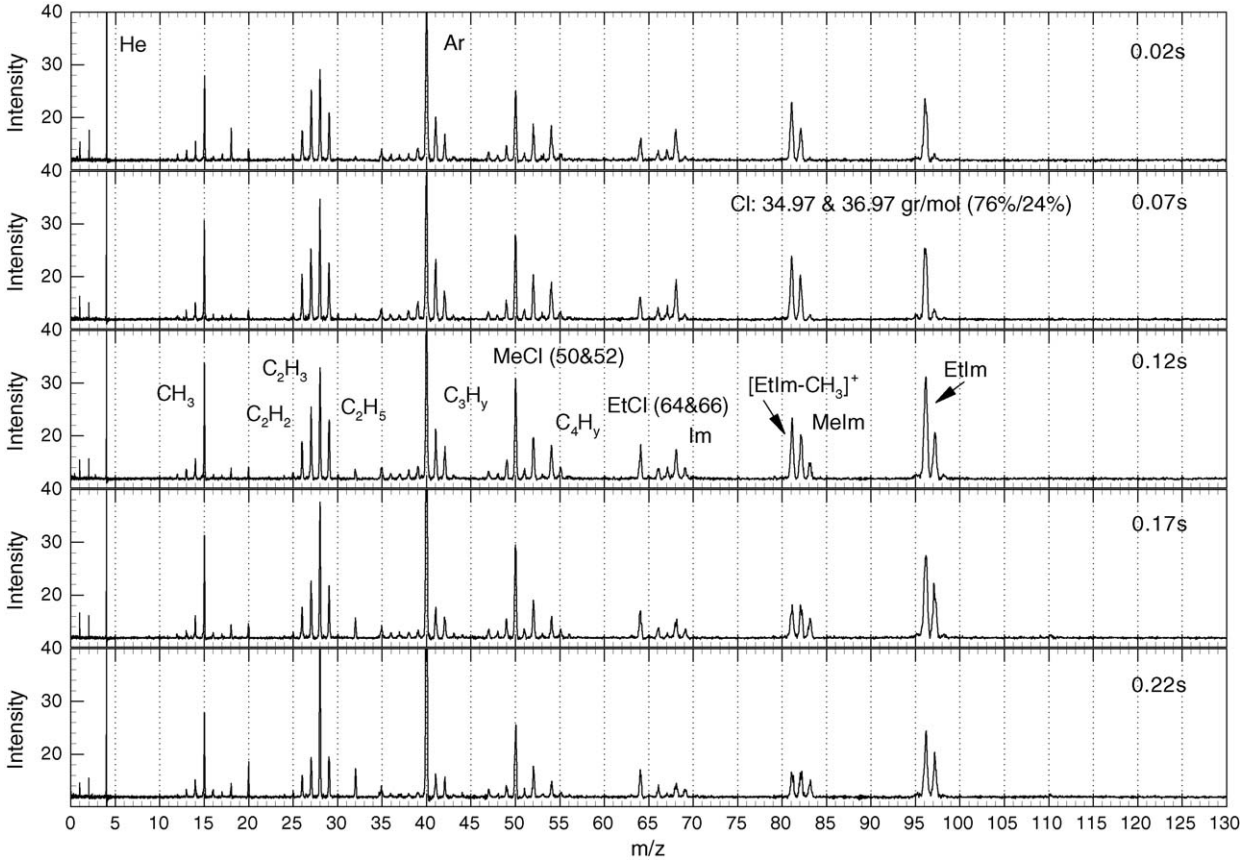

Fig. 7. Mass spectra from rapid thermolysis of [emim]Cl at 420 °C and 1 atm Ar, He and residual air extracted at 0.02, 0.07, 0.12, 0.17, 0.22 s (average of 10 spectra).

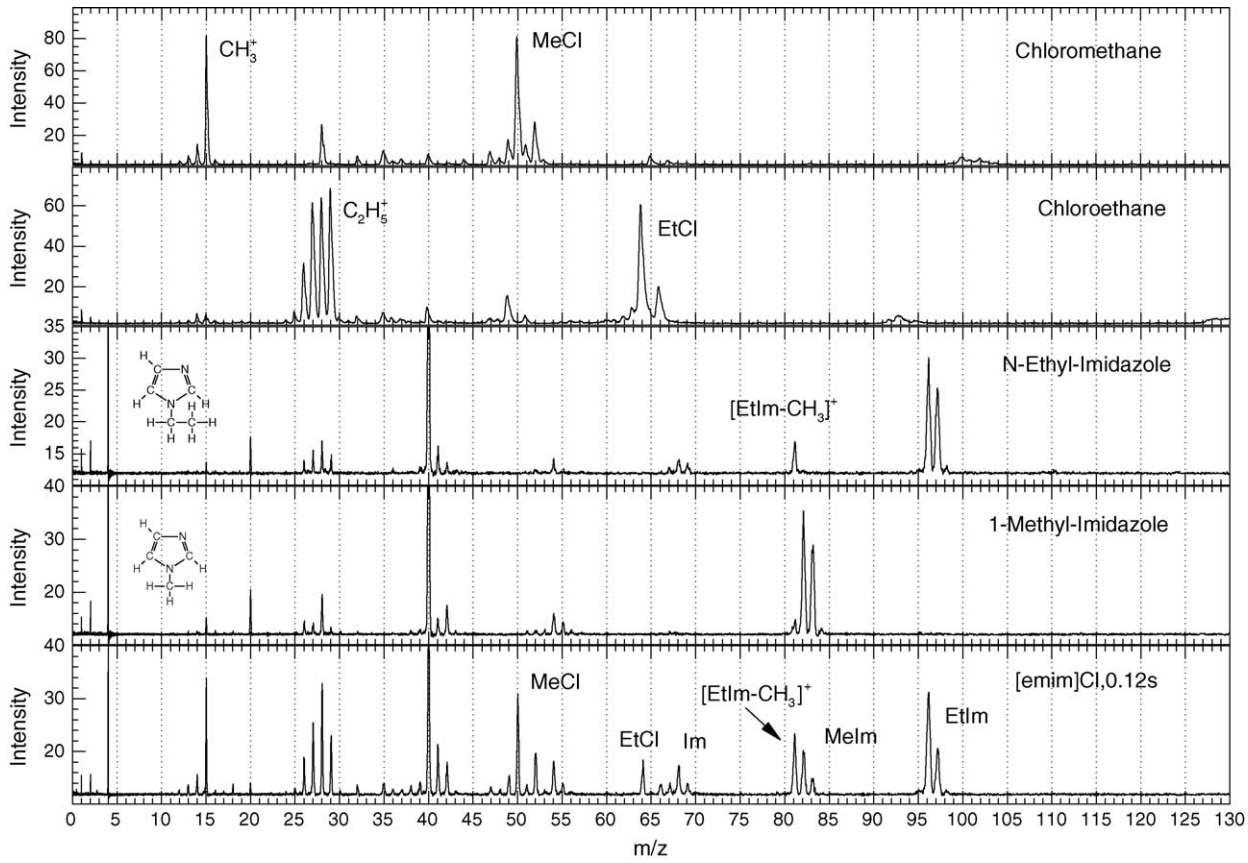

Fig. 8. Mass spectra of [emim]Cl, 1-MeIm, *N*-EtIm, chloroethane and chloromethane for identification of thermolysis products.

way involves the formation of EtCl and 1-MeIm. Proton transfer does not occur directly to form HCl, which is a highly IR-active species.

To verify the above findings using FTIR spectroscopy, results from ToF spectrometry are shown in Figs. 7 and 8. Averaging 10 consecutive spectra was found to provide a high degree of accuracy with the standard deviation of the intensities staying below a value of 5 units. The standard deviation at $m/z = 96$ at 0.02 s for [emim]Cl was found to be 3.7. The mass spectra in Figs. 7 and 8 appear at a first glance as quite complicated due to the fact that a high ionisation potential is used. However, the use of such high ionization potential allows comparison with available mass spectral data bases for a wide range of chemical compounds. Fig. 7 shows that the evolution of various species initially occurs at a fast rate, and then decays quickly. A closer inspection reveals the abundance of EtIm at $m/z = 96$ over MeIm at $m/z = 82$. Examination of the m/z spectrum for MeCl in Fig. 8 shows that the fragmented charged species include largely the CH_3^+ group and is thus the major contributor to $m/z = 15$ for [emim]Cl. The fragmentation of 1-MeIm also produces the CH_3^+, but to a much smaller extent compared to MeCl. The fragmentation of EtCl produces to a large extent many of the hydrocarbon ions near $m/z = 28$; that is, the charge is largely carried with the ethyl group, and to a much smaller extent with the chlorine ion near $m/z = 35$ or 37. Ionization of *N*-EtIm also produces charged species near $m/z = 28$, but also large ions at $m/z = 68$ and 81, corresponding to a loss of C_2H_4 and CH_3 groups, respectively. The appearance of $m/z = 54$, 52, 42 and 41 suggests that the ring does fracture as well, largely due to the high ionization potential. The scope of this work does not permit detailed discussion of the fragmentation pathways, but the reader is directed to similar works [42]. Additionally, the mass spectra acquired by the ToF mass spectrometer of MeCl, EtCl and 1-MeIm are in excellent agreement of those listed in the NIST data base [37]. Finally, metastable peaks are lacking in the spectra shown [43].

With the availability ToF mass spectra shown in Figs. 7 and 8, the thermolysis behavior [emim]Cl is quite clear; the dominant pathway involves the methyl group to form MeCl and *N*-EtIm. There is an abundance of CH_3^+ and MeCl at $m/z = 50$ and 52, and there is an abundance of *N*-EtIm, 1-Im, $m/z = 81$, as well as $m/z = 26$–29.

Figs. 9 and 10 show several ToF mass spectra from the rapid thermolysis of [emim]Br. Although not included here, the FTIR spectra are strikingly similar to those obtained from thermolysis of [emim]Cl. Inspection of Figs. 9 and 10 reveals that proton transfer does not occur to form HBr, but instead the decomposition pathways are equivalent to those of [emim]Cl. Here we include MeBr and EtBr mass spectra from the NIST database [37]. Close review of the mass spectra and comparison with [emim]Cl reveals that the only changes in m/z positions are those associated with Br-containing charged species.

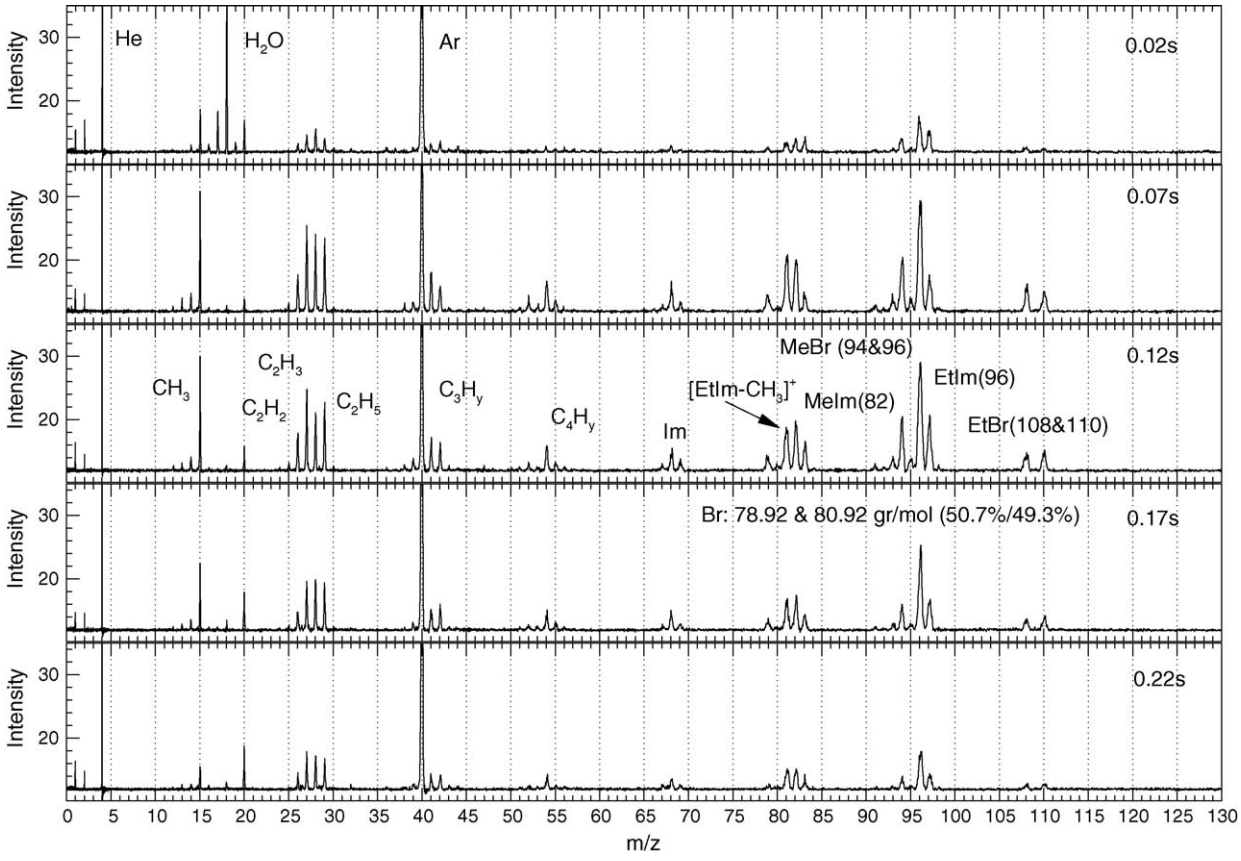

Fig. 9. Mass spectra from rapid thermolysis of [emim]Br at 420 °C and 1 atm Ar, He and residual air extracted at 0.02, 0.07, 0.12, 0.17, 0.22 s (average of 10 spectra).

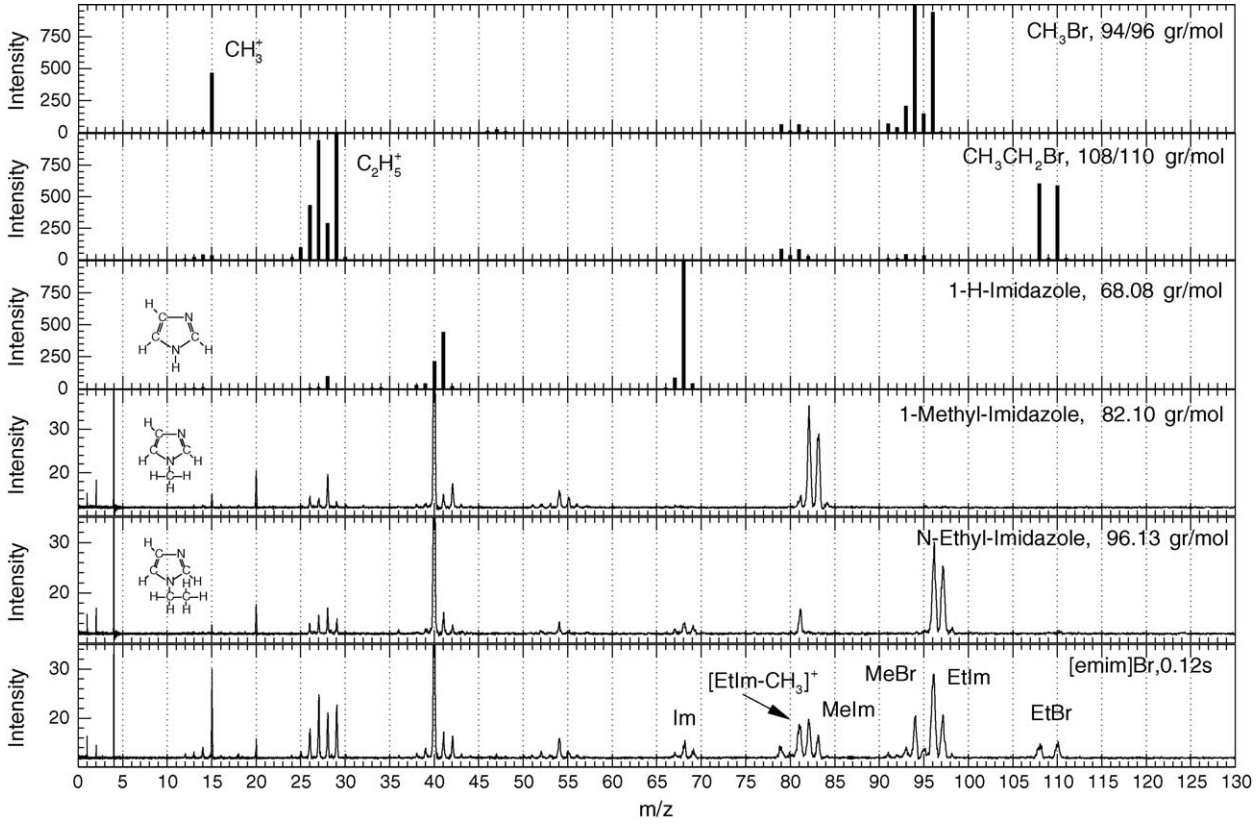

Fig. 10. Mass spectra of [emim]Br, *N*-EtIm, 1-MeIm, imidazole, C_2H_5Br and CH_3Br for identification of thermolysis products.

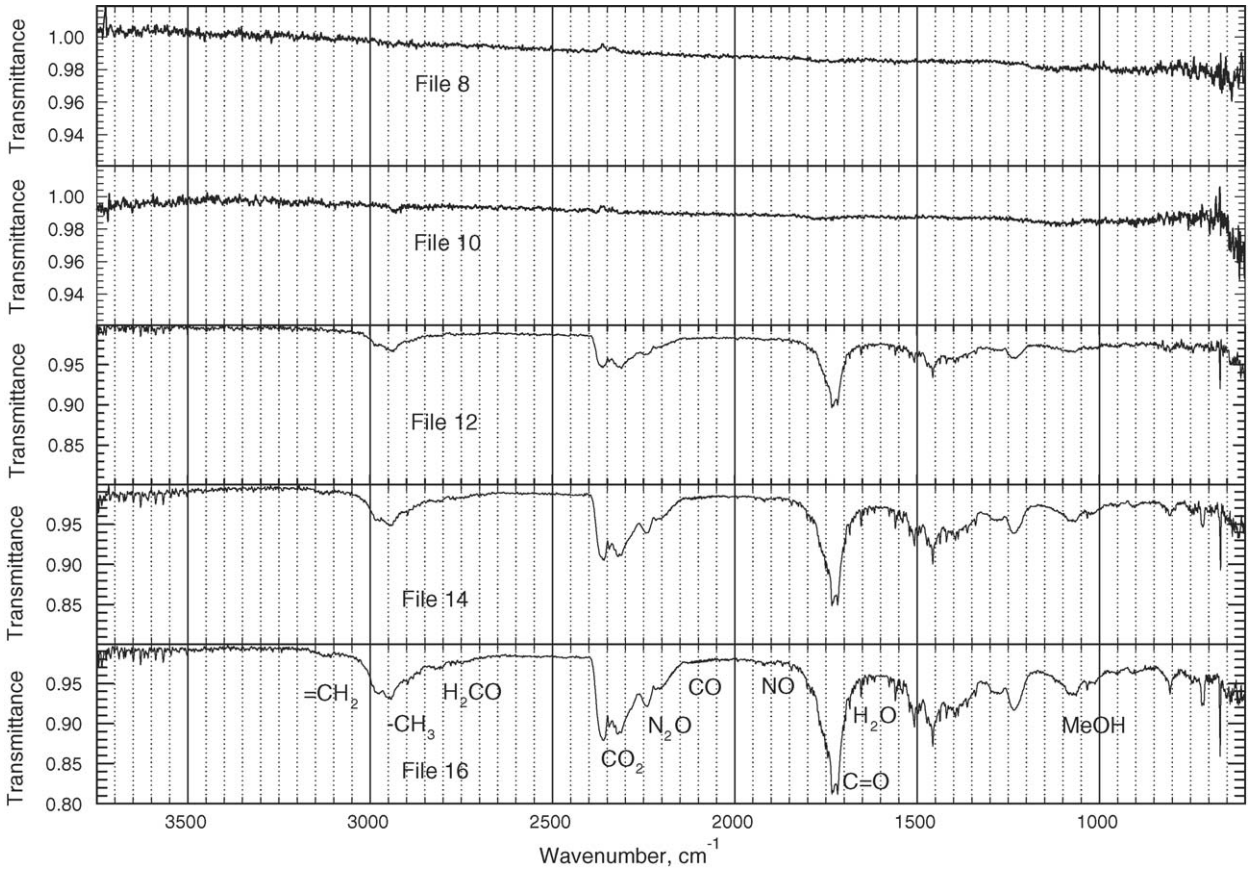

Fig. 11. FTIR spectra showing the evolution of species from rapid thermolysis of [emim]NO_3 at 435 °C and 1 atm N_2.

3.2. Thermal decomposition of [emim]NO_3

[emim]NO_3 is a stable crystalline, hygroscopic solid under standard conditions, with a melting point of 39 °C and a boiling point of around 300 °C. Rapid thermolysis, defined by almost complete decomposition of the material in less than 5 s, was achieved above temperatures of 390 °C. A small amount of a carbonaceous residue remains on the aluminum foil.

Fig. 11 shows five consecutive spectra during rapid thermolysis of [emim]NO_3. The spectra were taken in time intervals of 50 ms at a temperature of 435 °C and pressure of 1 atm. The evolution of products started with the 12th spectrum, which was approximately 0.1 s into the event. The rovibrational modes of various gaseous molecules that are easily identifiable in the spectra are listed in Table 2. Strong absorption bands of H_2O, CO_2, CO, NO, N_2O, CH_3OH and species containing a C=O bond are marked on the 16th spectrum. Aldehydes and ketones normally show strong features in the range from 1700 to 1750 cm^{-1}. H_2CO is also present, as its rovibrational features near 2700 cm^{-1} are visible. The spectra also contained the rovibrational bands seen in the spectra from 1-MeIm and *N*-EtIm. The presence of lines in the region 3500–3750 and 1595 cm^{-1} was in part due to atmospheric water vapor in the background, which could not be completely eliminated due to high humidity levels in the laboratory. Additionally, the N–H stretch near 3500 cm^{-1} is absent.

Fig. 12 is a superposition of spectra obtained from thermolysis of [emim]NO_3 at 435 °C, 1 atm in a N_2 environment, 1-MeIm at 281 °C, 1 atm, *N*-EtIm and 1-Im. While comparing the spectra, the broadening of individual bands due to the elevated temperature of decomposition of [emim]NO_3 is evident. From 2800 to 3200 cm^{-1}, there is a noticeable agreement in the =C–H stretch and the C–H stretch in the $-CH_3$ group between the spectra. Two distinct bands for the C=C and C=N stretch from 1550 to 1400 cm^{-1} were easily recognizable. From 1300 to 1200 cm^{-1}, the frequencies for the C–N stretch and the C–H bip matched perfectly in the spectra. The C–N(1)–C bip with its prominent bands in 1100–1060 cm^{-1} and 930–880 cm^{-1} was noticeable.

Table 2
Frequency assignment for vibrational modes for gaseous products formed in the decomposition of [emim]NO_3 at 435 °C, 1 atm in a N_2 environment

Description	Frequency (cm^{-1})	Comments
H_2O	3500–3750, 1565–1650	Atmospheric H_2O leads to uncertainty
HCN	700–725	
H_2CO	2740–3940, 1680–1750	Weak absorption bands
CO_2	3500–3750, 2320–2380	Strong absorption band
N_2O	2140–2250	
CO	2140–2250	
NO	1880–2140	
CH_3OH	950–1085	

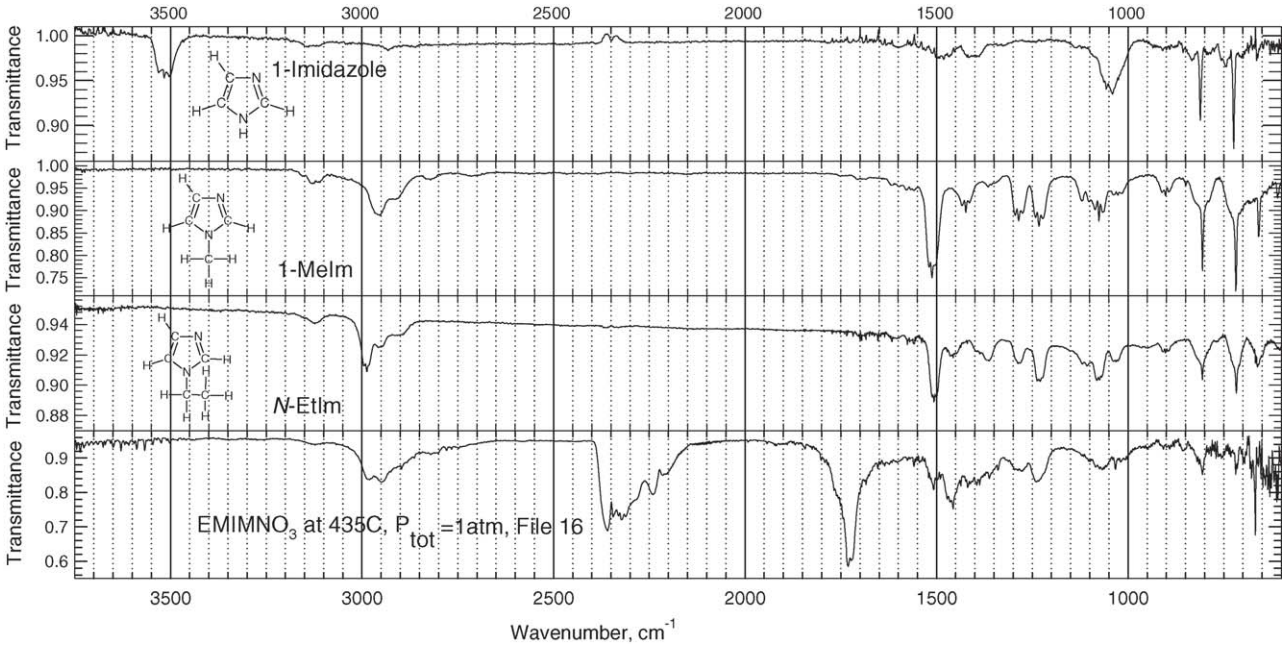

Fig. 12. FTIR spectra of [emim]NO_3, *N*-EtIm, 1-MeIm and imidazole for identification of thermolysis products.

In addition, two C–H bop frequency bands around 800 and 730 cm^{-1} were detected. The striking similarity between the spectra corroborated the formation of 1-MeIm and *N*-EtIm as products during thermolysis of [emim]NO_3. There are some differences in the details of the individual bands. These differences are attributed to the presence of a wide range of smaller molecular weight species in the gas-phase region in the case of thermolysis of [emim]NO_3 causing broadening of lines, whereas broadening of lines of 1-MeIm is caused by N_2 and by 1-MeIm itself.

Results from the use of the ToF MS provide additional details on the rapid thermolysis behavior of [emim]NO_3. Fig. 13 shows the temporal evolution of *m/z* spectra acquired at 1000 Hz, and averaging often spectra. Hence, the temporal resolution is 0.01 s. Examination of Fig. 13, along with Fig. 14, reveals that proton transfer is likely to primarily involve the methyl group for two reasons. First, the extent of *N*-EtIm evolved is relatively large compared to 1-MeIm. Second, the extent of ionized CH_3^+ is relatively small. Third, subsequent reactions near the methyl group produces *m/z* = 126, which is believed to be a methoxy-EtIm, involving H-abstraction from the C(2), C(4) or C(5) carbon on the ring. The methoxy itself is an intermediate that may also abstract H-atoms from other hydrocarbons, forming in part the small amount of MeOH that is detected. Fragmentation of this molecule yields the methoxy-MeIm as well as the methoxy-Im. Species near *m/z* = 28 originate largely from fragmentation of *N*-EtIm, since HCN formation due to ring fracture is absent from the FTIR spectra; a strong peak at 712 cm^{-1} would otherwise be visible. Additionally, the peaks at *m/z* = 56, 57 and 58 are likely caused by various aldehydes including acrolein $H_2CCHCHO$ at *m/z* = 56 and propionaldehyde H_3CCH_2CHO at *m/z* = 58. Fragmentation of these aldehydes produces an appreciable fraction of the charged species in the range from *m/z* = 25 to 30, but the parent molecule is also detected by the TOFMS.

3.3. Decomposition pathways of [emim]NO_3

The complex structure of [emim]NO_3 and the extent of secondary reactions within the condensed phase make the prediction of the initial chemical kinetic steps under high temperatures a challenging task. Based on the results from decomposition of [emim]Br and [emim]Cl, the pathways are likely to involve the same initial steps. That is, proton transfer yields:

$$[\text{emim}]NO_3 \rightarrow CH_3ONO_2 + N\text{-EtIm} \quad (1)$$

It is the dominant pathway, with secondary steps initiated by:

$$CH_3ONO_2 \rightarrow \begin{array}{l} CH_3O + NO_2 \\ CH_3O + NO_2 \rightarrow CH_2O + HONO \end{array}$$

H-atom abstraction from one of the carbon atoms (e.g. from C(2)) on the ring follows quickly to yield the detected 1-ethyl-2-methoxy-1*H*-imidazole (EtMeOIm) at *m/z* = 126

$$NO_2 + N\text{-EtIm} \rightarrow HONO + \text{1-ethyl-1}H\text{-imidazol-2-yl}$$

$$CH_3O + \text{1-ethyl-1}H\text{-imidazol-2-yl} \rightarrow \text{EtMeOIm}$$

The carbon atom to which the methoxy is attached is not certain. Subsequent reactions between methoxy and nitrate also occur, to produce the detected water vapor, nitrous oxide, nitric oxide, methanol, carbon monoxide and dioxide. Detailed discussions of those are beyond the scope of this paper, and are generally contained in larger reaction mechanisms discussed by many authors, including gas-phase reactions [44,45] as well as condensed-phase reactions with consideration to the cage effect [46].

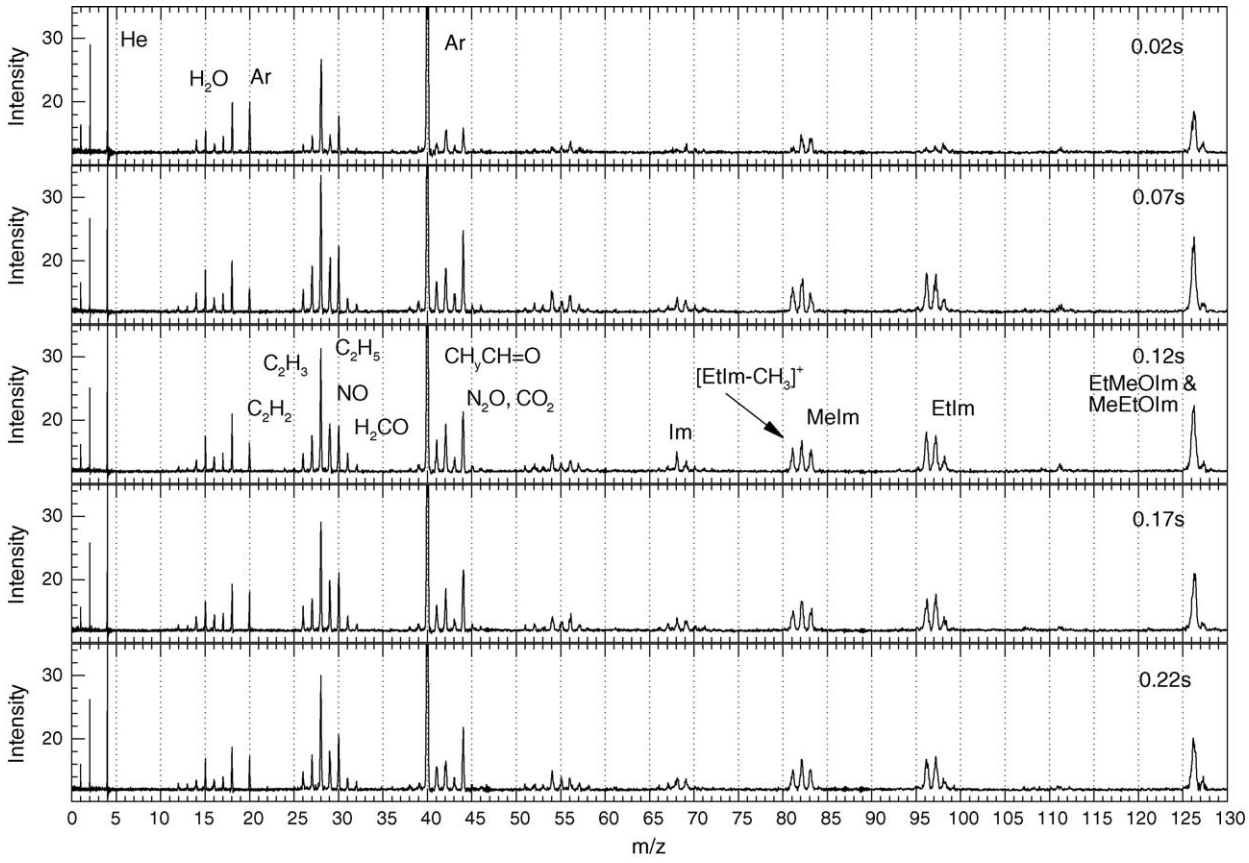

Fig. 13. Mass spectra from rapid thermolysis of [emim]NO_3 at 420 °C and 1 atm Ar, He and residual air extracted at 0.02, 0.07, 0.12, 0.17, 0.22 s (average of 10 spectra).

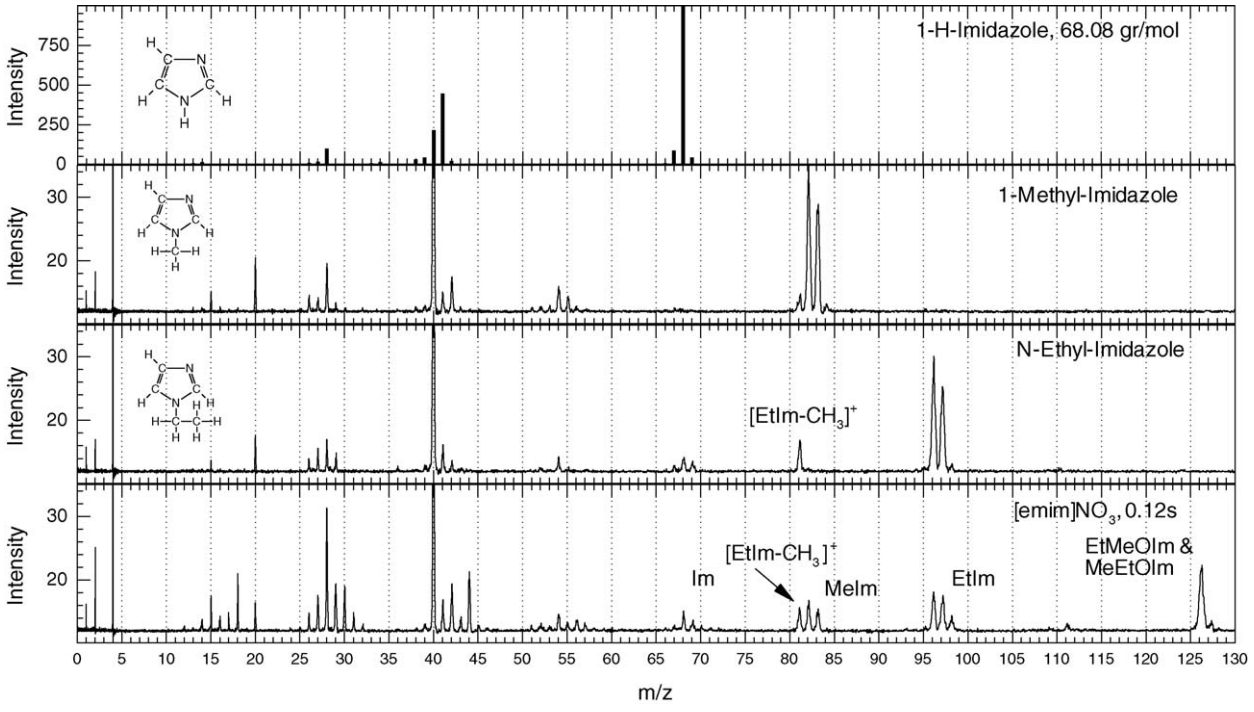

Fig. 14. Mass spectra of [emim]NO_3, *N*-EtIm, 1-MeIm and imidazole for identification of thermolysis products.

The second and less important pathway involves proton transfer of the ethyl group:

$$[\text{emim}]NO_3 \rightarrow C_2H_5ONO_2 + \text{1-MeIm} \quad (2)$$

A wide variety of secondary steps take place, but products detected in the gas-phase having a large molecular weight include the aldehydes, which are believed to be at $m/z = 44$, 56, 57 and 58 as well as the strong presence of the C=O band at 1730 cm^{-1}. Important steps include:

$$C_2H_5ONO_2 \rightarrow C_2H_5O + NO_2$$
$$C_2H_5O + NO_2 \rightarrow CH_3CHO + HONO$$

A similar H-atom abstraction from a carbon atom on the ring (e.g. from C(2)) yields 1-methyl-2-ethoxy-1*H*-imidazole (MeEtOIm), with the same m/z value as 1-ethyl-2-methoxy-1*H*-imidazole (EtMeOIm).

$$NO_2 + \text{1-MeIm} \rightarrow HONO + \text{1-methyl-1}H\text{-imidazol-2-yl}$$

$$C_2H_5O + \text{1-methyl-1}H\text{-imidazol-2-yl} \rightarrow \text{MeEtOIm}$$

It is believed that HNO_3, by deprotonation form C(2), C(4), or C(5), is not formed since some of it would be detected by the FTIR due to its strong IR-activity; ToFMS does not readily detect the HNO_3, however [47].

The preferential proton transfer between the methyl group and the nitrate group over the ethyl group and the nitrate group needs further elucidation. Molecular dynamics simulations by Voth et al. [48,49] using 216 ionic pairs and under working conditions of atmospheric pressure and 400 K showed that $[\text{emim}]NO_3$ was a strongly coupled ionic system with nitrate anions concentrated around the highly positive C(2)–H(2) bond. A closer inspection revealed that the nitrate ions reside nearer to the methyl group compared to the ethyl group. A study of [emim]Cl using ab initio techniques by Turner et al. [50] suggested that the chloride anion, located in the plane of the ring was located in the vicinity of the methyl group. However, a similar study on [emim]Br revealed that the bromide anion was most stable above the plane of the ring. Despite conducted at lower temperatures, these simulations of the most stable structures of $[\text{emim}]NO_3$ and [emim]Cl may provide information on the potential or most probable location of the atoms or molecular groups involved in the initial reaction steps in the condensed phase.

4. Conclusions

Rapid thermolysis studies have been carried out on three imidazolium-based ionic liquids. Using FTIR spectroscopy and ToF mass spectrometry as the diagnostic tools, an analysis of the evolved species has shown that proton transfer involves primarily the methyl group and secondarily the ethyl group, whereas the ring remains largely intact although the temperatures employed reached 435 °C. The formed species after proton transfer involving $[\text{emim}]NO_3$ are extremely reactive and produce small molecular weights products at a high rate. Studies involving [emim]Br and [emim]Cl produced no evidence of either HBr or HCl, both of which are strongly IR-active. Besides evidence of the formation of 1-MeIm and *N*-EtIm for the two latter ionic liquids, the proton transfer yields hydrocarbons containing methyl and ethyl groups. Further decomposition of the hydrocarbon halides is not evident.

Acknowledgments

This material is based upon work supported by the U.S. Air Force Office of Scientific Research under Contract No. F49620-03-1-0211, with Dr. Michael Berman serving as the program manager. Funding for the purchase of the time-of-flight mass spectrometer by the U.S. Army Research Office under Contract No. DAAD19-01-1-0449, with Dr. David M. Mann serving as the program manager, is gratefully acknowledged.

References

[1] P. Walden, Bull. Acad. Imper. Sci. (St. Petersburg) (1914) 1800.
[2] R.J. Gale, B. Gilbert, R.A. Osteryoung, Inorg. Chem. 17 (1978) 2728–2729.
[3] J.S. Wilkes, Green Chem. 4 (2002) 73–80.
[4] A.A. Fannin, D.A. Floreani, L.A. King, J.S. Landers, B.J. Piersma, D.J. Stech, R.L. Vaughn, J.S. Wilkes, J.L. Williams, J. Phys. Chem. 88 (1984) 2614–2627.
[5] J.S. Wilkes, M.J. Zaworotko, J. Chem. Soc., Chem. Commun. (1992) 965–967.
[6] J.D. Holbrey, K.R. Seddon, Clean Products Processes 1 (4) (1999) 223–236.
[7] A.S. Larsen, J.D. Holbrey, F.S. Tham, C.A. Reed, J. Am. Chem. Soc. 122 (2000) 7265–7272.
[8] J.S. Wilkes, J.A. Levisky, R.A. Wilson, C.L. Hussey, Inorg. Chem. 21 (3) (1982) 1263–1264.
[9] J. Sun, M. Forsyth, D.R. MacFarlane, J. Phys. Chem. B 102 (44) (1998) 8858–8864.
[10] P. Bônhote, A.-P. Dias, N. Papageorgiou, K. Kalyanasundaram, M. Grätzel, Inorg. Chem. 35 (5) (1996) 1168–1178.
[11] J. Shah, J. Brennecke, E. Maginn, Green Chem. 4 (2002) 112–118.
[12] M.J. Earle, K.R. Seddon, Pure Appl. Chem. 72 (7) (2000) 1391–1398.
[13] T. Welton, Chem. Rev. 99 (1999) 2071–2083.
[14] C.M. Gordon, Appl. Catal. A 222 (2001) 101–117.
[15] J. Dupont, R.F. de Souza, P.A.Z. Suarez, Chem. Rev. 102 (10) (2002) 3667–3692.
[16] H. Olivier-Bourbigou, L. Magna, J. Mol. Catal. A: Chem. 182–183 (2002) 419–437.
[17] S. Trohalaki, R. Pachter, G.W. Drake, T. Hawkins, Energy Fuels 19 (2005) 279–284;
G.W. Drake, T.W. Hawkins, L.A. Hall, J.A. Boatz, A.J. Brand, Propellants, Explos., Pyrotech. 30 (2005) 329–337;
G. Drake, T. Hawkins, A. Brand, L. Hall, M. Mckay, A. Vij, I. Ismail, Propellants, Explos., Pyrotech. 28 (2003) 174–180.
[18] J.L. Anthony, E.J. Maginn, J.F. Brennecke, J. Phys. Chem. B 105 (44) (2001) 10942–10949.
[19] J.L. Anthony, E.J. Maginn, J.F. Brennecke, J. Phys. Chem. B 106 (29) (2002) 7315–7320.
[20] J.J. Jardine, B.A. Patterson, M.L. Origlia-Luster, E.M. Woolley, J. Chem. Thermodyn. 34 (6) (2002) 895–913.
[21] H.L. Ngo, K. Lecompte, L. Hargens, A.B. McEwen, Thermochim. Acta 357–358 (2000) 97–102.
[22] P. Naumov, V. Jordanovska, B. Boyanov, G. Jovanovski, J. Therm. Anal. Calorim. 66 (2) (2001) 469–477.
[23] J.W. Gilman, W.H. Awad, R.D. Davis, J. Shields, R.H. Harris Jr., C. Davis, A.B. Morgan, T.E. Sutto, J. Callahan, P.C. Trulove, H.C. Delong, Chem. Mater. 14 (9) (2002) 3776–3785.

[24] M. Egashira, S. Okada, J.-I. Yamaki, Solid State Ionics 148 (3–4) (2002) 457–461.
[25] C.R. Bhattacharjee, P.K. Choudhury, Transition Met. Chem. 23 (5) (1998) 561–564.
[26] E.M. Abd Alla, M.I. Abdel-Hamid, J. Therm. Anal. Calorim. 62 (3) (2000) 769–780.
[27] B.K.M. Chan, N.-H. Chang, M.R. Grimmett, Aust. J. Chem. 30 (1977) 2005–2013.
[28] K.J. Baranyai, G.B. Deacon, D.R. MacFarlane, J.M. Pringle, J.L. Scott, Aust. J. Chem. 57 (2004) 145–147.
[29] L. Minier, R. Behrens Jr., S. Bulusu, Decomposition, Combustion and Detonation Chemistry of Energetic Materials, M.R.S. Symposium Proceedings 418 (1996) 111–117.
[30] H. Xue, S.W. Arritt, B. Twamley, J.M. Shreeve, Inorg. Chem. 43 (25) (2004) 7972–7977.
[31] H. Xue, Y. Gao, B. Twamley, J.M. Shreeve, Chem. Mater. 17 (1) (2005) 191–198.
[32] Y. Gao, S.W. Arritt, B. Twamley, J.M. Shreeve, Inorg. Chem. 44 (14) (2005) 5068–5072.
[33] G. Fischer, G. Holl, T.M. Klapötke, J.J. Weigand, Thermochim. Acta 437 (2005) 168–178.
[34] Y. Dessiaterik, T. Baer, R.E. Miller, J. Phys. Chem. A (2005) DOI: 10.1021/jp0532059.
[35] Y. Oyumi, T.B. Brill, Comb. Flame 62 (3) (1985) 233–241;
G.K. Williams, T.B. Brill, Combust. Flame 102 (1995) 418–426;
T.B. Brill, H. Ramanathan, Combust. Flame 122 (2000) 165–171.
[36] E.S. Kim, H.S. Lee, C.F. Mallery, S.T. Thynell, Combust. Flame 110 (1997) 239–255.
[37] P.J. Linstrom, W.G. Mallard (Eds.), NIST Chemistry WebBook, NIST Standard Reference Database Number 69, June 2005, National Institute of Standards and Technology, Gaithersburg MD, 20899 (http://webbook.nist.gov).
[38] W. Tatara, M.J. Wójcik, J. Lindgren, M. Probst, J. Phys. Chem. A 107 (2003) 7827–7831.
[39] J. Sadlej, A. Jaworski, K. Miaskiewicz, J. Mol. Struct. 274 (1992) 247–257.
[40] G. Socrates, Infrared and Raman Characteristic Group Frequencies, Wiley, Chichester, England, 2001.
[41] N. Capon, R.A. Ross, Trans. Faraday Soc. 62 (1966) 1560–1566;
K.A. Holbrook, A.R.W. Marsh, Trans. Faraday Soc. 63 (1967) 643–654;
J.R. Christie, W.D. Johnson, A.G. Loudon, A. MacColl, M.N. Mruzek, J. Chem. Soc., Faraday Trans. 1 (1975) 1937–1942.
[42] M. Ohashi, N. Ohno, H. Kakisawa, Org. Mass Spectrom. 1 (1968) 703–712;
J.V. Thuijl, K.J. Klebe, J.J.V. Houte, Org. Mass Spectrom. 7 (1973) 1165–1172.
[43] F.W. McLafferty, Interpretation of Mass Spectra, University Science Books, California, USA, 1993.
[44] R.A. Yetter, F.L. Dryer, M.T. Allen, J.L. Gatto, J. Prop. Power 11 (4) (1995) 683–697.
[45] Y.-X. Zhang, S.H. Bauer, Int. J. Chem. Kinet. 31 (9) (1999) 655–673.
[46] C.F. Melius, M.C. Piqueras, Int. Symp. Combust. 29 (2) (2002) 2863–2870.
[47] C.S.S. O'Connor, N.C. Jones, S.D. Price, Int. J. Mass Spectr. Ion Proc. 163 (1997) 131–139.
[48] M.G. Del Pópolo, G.A. Voth, J. Phys. Chem. B 108 (2004) 1744–1752.
[49] T. Yan, C.J. Burnham, M.G. Del Pópolo, G.A. Voth, J. Phys. Chem. B 108 (32) (2004) 11877–11881.
[50] E.A. Turner, C.C. Pye, R.D. Singer, J. Phys. Chem. A 107 (2003) 2277–2288.